Editors' Suggestion

## Manipulation of Coupling and Magnon Transport in Magnetic Metal-Insulator **Hybrid Structures**

Yabin Fan,<sup>1,\*,‡</sup> P. Quarterman<sup>®</sup>,<sup>2,†,‡</sup> Joseph Finley,<sup>1</sup> Jiahao Han,<sup>1</sup> Pengxiang Zhang,<sup>1</sup> Justin T. Hou,<sup>1</sup> Mark D. Stiles, Alexander J. Grutter, and Lugiao Liu<sup>1</sup>

<sup>1</sup>Microsystems Technology Laboratories, Massachusetts Institute of Technology, Cambridge, Massachusetts 02139, USA

<sup>&</sup>lt;sup>3</sup>Physical Measurement Laboratory, National Institute of Standards and Technology, 100 Bureau Drive, Gaithersburg, Maryland 20899, USA



(Received 9 March 2020; accepted 1 May 2020; published 15 June 2020)

Ferromagnetic metals and insulators are widely used for generation, control, and detection of magnon spin signals. Most magnonic structures are based primarily on either magnetic insulators or ferromagnetic metals, while heterostructures integrating both of them are less explored. Here, by introducing a Pt/yttrium iron garnet (YIG)/permalloy (Py) hybrid structure grown on a Si substrate, we study the magnetic coupling and magnon transmission across the interface of the two magnetic layers. We find that within this structure, Py and YIG exhibit an antiferromagnetic coupling field as strong as 150 mT, as evidenced by both magnetometry and polarized neutron reflectometry measurements. By controlling individual layer thicknesses and external fields, we realize parallel and antiparallel magnetization configurations, which are further utilized to control the magnon current transmission. We show that a magnon spin valve with an on:off ratio of approximately 130% can be realized out of this multilayer structure at room temperature through both spin pumping and spin-Seebeck-effect experiments. Owing to the efficient control of magnon current and the compatibility with Si technology, the Pt/YIG/Py hybrid structure could potentially find applications in magnon-based logic and memory devices.

DOI: 10.1103/PhysRevApplied.13.061002

Heterostructures that integrate magnetic insulators and ferromagnetic metals are drawing widespread attention due to their rich magnonic physics. Specifically, standing spin waves (SSWs) and interlayer magnon-magnon coupling have been detected in such hybrid structures [1– 3], with coupled layers of the magnetic insulator yttrium iron garnet (YIG) and a soft ferromagnetic metal [such as Co, (Co,Fe)B, and Ni]. In these structures, the dynamic torques generated from interlayer exchange coupling can lead to anticrossings between magnon modes unlocking functionalities with critical implications both in the classical [4,5] and quantum domains [1-3,6]. In addition to magnon-magnon coupling, the interlayer exchange interaction in YIG/ferromagnetic metal bilayers can enable additional magnonic functions [7] such as the magnon spin-valve effect [8,9]. In magnon spin valves, the transmission coefficient of magnons propagating through the heterostructure is tuned by the parallel and antiparallel orientations between the magnetization of two magnetic layers. One advantage of such a magnonic spin-valve device is that information is encoded in the form of magnons and a net charge current is not required in principle, avoiding Joule-heating-related dissipation in conventional spin-valve structures. In existing studies, YIG layers epitaxially grown on Gd<sub>3</sub>Ga<sub>5</sub>O<sub>12</sub> (GGG) substrate are generally utilized. However, for practical device applications, spin-valve structures grown on silicon substrates are preferred [10,11]. Stronger coupling between YIG and ferromagnetic metals may provide easier customization of the magnetization orientation in the magnon spin-valve structures.

In this work, we demonstrate strong magnetic coupling in the Si/Pt/YIG/permalloy (Py) multilayer structures. We show that a pronounced antiferromagnetic coupling exists between polycrystalline YIG and Py layers in the lowfield regime (defined as 0 to 50 mT), with the two layers aligning along the same direction only when the external field exceeds 150 mT. Moreover, through spin-pumping and spin-Seebeck experiments, we demonstrate that this YIG/Py hybrid structure could serve as an efficient magnon spin valve. The YIG/Py hybrid structures grown on Si

<sup>&</sup>lt;sup>2</sup>NIST Center for Neutron Research, National Institute of Standards and Technology, 100 Bureau Drive, Gaithersburg, Maryland 20899, USA

<sup>\*</sup>yabin fan@hotmail.com

<sup>†</sup>patrick.quarterman@nist.gov

<sup>&</sup>lt;sup>‡</sup>These authors contributed equally to this work.

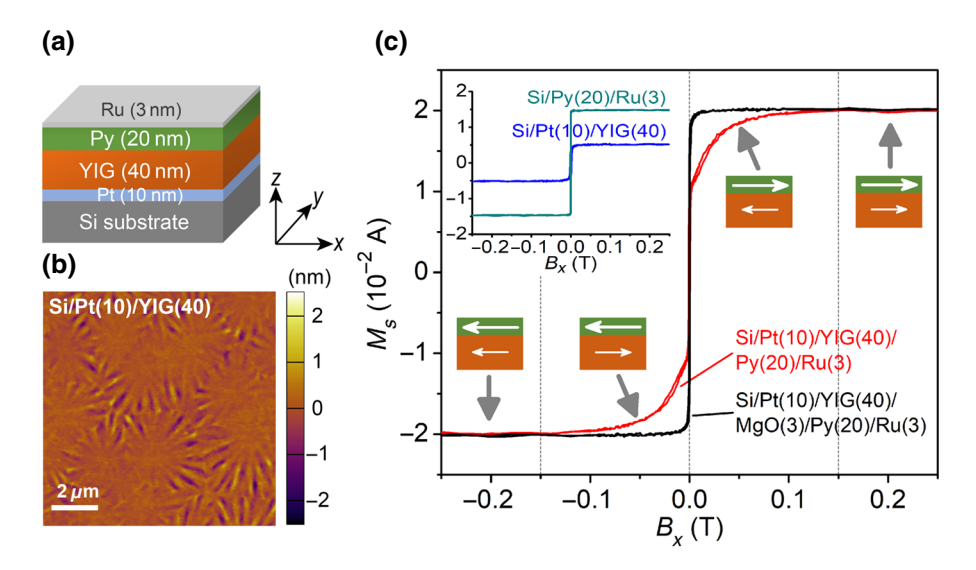


FIG. 1. (a) Schematic of the Pt(10)/YIG(40)/Py(20)/Ru(3) hybrid structure grown on the Si/SiO<sub>2</sub> substrate. (b) Atomic force microscopy image of the YIG surface for the Si/Pt(10)/YIG(40) film, indicating a roughness of around 1 nm. (c) Vibrating sample magnetometry measurements of the Si/Pt(10)/YIG(40)/Py(20)/Ru(3) sample and Si/Pt(10)/YIG(40)/MgO(3)/Py(20)/Ru(3) sample. The inset shows results from the control samples of Si/Py(20)/Ru(3) and Si/Pt(10)/YIG(40). Schematics show the magnetization orientation of the YIG and Py layers in the Si/Pt(10)/YIG(40)/Py(20)/Ru(3) hybrid structure in different magnetic field regions.  $M_s$  is integrated over the multilayer thickness.

represent a semiconductor industry-compatible technique for implementing magnonic spin valves and thus have broad application in ultralow-power magnonic devices and circuits.

We first deposit Pt(10)/YIG(40) thin films (units in nanometers) on Si/SiO<sub>2</sub> substrates by magnetron sputtering [12–15], followed by rapid thermal annealing (RTA) in an oxygen environment. To characterize the film quality, atomic force microscopy (AFM) measurements are performed [Fig. 1(b)], which indicate a surface roughness of approximately 1 nm. The polycrystalline nature of the YIG layer is verified by x-ray diffraction (Fig. S1 within the Supplemental Material) [16]. After annealing, a 20-nm Py thin film is grown on top of the YIG layer, followed by a 3-nm Ru passivation layer [see Fig. 1(a)].

To characterize the magnetic properties of the hybrid structure, we collect vibrating sample magnetometry (VSM) data at room temperature with magnetic fields applied within the sample plane. As shown in Fig. 1(c), the M-H curve of the Pt/YIG/Py sample shows segmented switching features. After the magnetization sharply switches polarity near  $B_x = 0$  T, it does not immediately reach the saturated magnetization state. Instead, it gradually increases, reaching saturation at around  $B_r = 150$  mT. In order to understand this peculiar behavior, we measure a set of control samples. For the control samples of Py(20) and Pt(10)/YIG(40), the M-H curves exhibit typical easy-axis hysteresis loops with low coercive field and square switching shape (the ratio of remanent over saturation magnetization,  $M_r/M_s \approx 1$ ), as plotted in the inset of Fig. 1(c). Comparing the magnetization of these three

samples, we find that in the low-field region, the net magnetic moment  $M_{\text{total}}$  from the Pt/YIG/Py sample is equal to the value of M(Py)-M(YIG), suggesting antiferromagnetic coupling between these two layers. When the applied field is increased, the net moment  $M_{\text{total}}$  from the hybrid structure gradually increases until it reaches the sum of M(Py) and M(YIG) at approximately 150 mT, where both the Py and YIG magnetizations align with the field. To examine the detailed mechanisms of the observed antiferromagnetic coupling, we grew a control sample of Si/Pt(10)/YIG(40)/MgO(3)/Py(20), where the MgO layer serves as a spacer to prevent direct exchange coupling between the YIG and Py layers. In contrast to the Pt/YIG/Py sample, the M-H curve of this control sample shows full switching near  $B_x = 0$  T [Fig. 1(c)], which suggests that exchange interaction rather than the dipolar field is responsible for the observed coupling.

In order to directly measure the magnetization of individual layers, we used polarized neutron reflectometry (PNR) [17] to probe the depth dependence of the composition and in-plane magnetization. Figure 2(a) shows a typical set of PNR data obtained from the Si/Pt(10)/YIG(40)/Py(20) sample under 4 mT of external magnetic field (reached by first saturating to 700 mT and then lowering the field).  $R^{++}$  and  $R^{--}$  represent neutron reflectivity for the non-spin-flip channels and Q is the neutron-beam wave-vector transfer during the reflection. The solid lines represent theoretical reflectivity curves generated from the scattering length density depth profiles shown in Fig. 2(c). A series of data sets obtained under fields from 700 to 1.5 mT are illustrated in Figs. S2

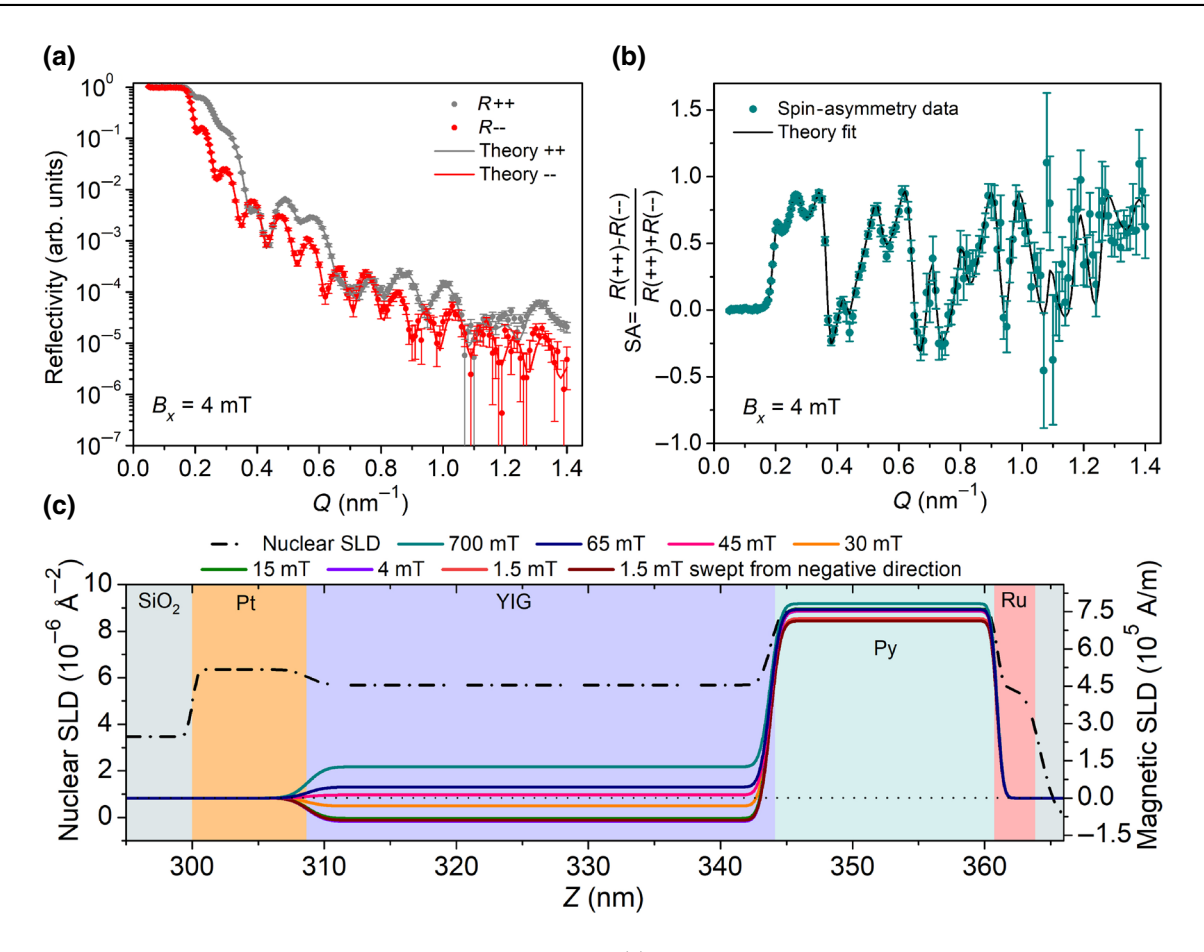


FIG. 2. (a) Polarized neutron reflectivity for the spin-polarized  $R^{++}$  and  $R^{--}$  channels. Points represent experimental results and solid lines are theoretical fits. Error bars indicate single standard deviation uncertainties. The results are obtained at room temperature with a 4 mT in-plane field. (b) Spin asymmetry between the two channels for data shown in (a). (c) Structural (nuclear) and magnetic scattering length density profiles for the multilayer structure under different in-plane field conditions.

and S3 within the Supplemental Material [16]. Figure 2(b) shows the calculated spin-asymmetry result, which is defined as  $SA = (R^{++} - R^{--})/(R^{++} + R^{--})$  and highlights the magnetic components of the reflectometry.

As described in the experimental methods section [16], we obtain the scattering length density (SLD) profiles [Fig. 2(c)], which provide information on the orientation and magnitude of in-plane magnetization as a function of depth from the sample surface. Under high fields, YIG and Py layers both align parallel to the applied field. Upon the reduction of applied magnetic field, the Py magnetization remains roughly unchanged while that from YIG decreases significantly. When the field is lowered to 15 mT, the magnetization of the YIG layer aligns such that approximately 70% of its saturated magnetization  $(M_s)$  is antiparallel to the magnetic field (and Py magnetization). The PNR results, including the onset field for YIG magnetization reversal as well as the relative magnitude of the magnetic moment of the different layers during the switching, are in good agreement with the M-H curve shown in Fig. 1(c).

We also use PNR to characterize the magnetization switching process on the control sample of Si/Pt(10)/YIG

(40)/MgO(3)/Py(20). Consistent with the VSM results, with MgO insertion, the YIG and Py layers remain aligned parallel to the applied magnetic field under both high-and low-field regimes in this sample (Fig. S5 within the Supplemental Material) [16], indicating the exchange interaction as the coupling mechanism in Si/Pt/YIG/Py.

In addition to the Si/Pt(10)/YIG(40)/Py(20) sample, whose net magnetization is dominated by the Py layer at low field, we also measure a sample of Si/Pt(10)/YIG(40)/Py(2)/Ru(4), in which the magnetic moment from YIG dominates. From both VSM and PNR measurements, we observe that in contrast to the Si/Pt(10)/YIG(40)/Py(20) sample, in this control sample the YIG magnetization remains parallel to the external inplane field, while the Py magnetization aligns opposite to the field direction in the low-field domain, as is shown in Fig. S4 within the Supplemental Material. The full PNR data with theoretical fits can be found in Sec. 4 within the Supplemental Material [16].

Previously the magnon spin-valve effect has been realized in magnetic multilayers. In these experiments, in order to isolate the coupling between two ferromagnetic layers

and allow both parallel and antiparallel configurations, an insertion layer made from an antiferromagnetic insulator or a paramagnetic metal [8,9] has been employed. Because of the intrinsic, antiferromagnetic coupling between the YIG and the Py layers, their relative magnetic orientation can be toggled between the two opposite states without the need for a spacer layer. We perform both spin-pumping and spin-Seebeck effect (SSE) measurements to study the modulation on magnon current transport in this hybrid structure [Figs. 3(b) and 3(d)].

As shown in Fig. 3(a), a spin-pumping device is fabricated out of the Si/Pt(10)/YIG(40)/Py(20)/Ru(3) stack with electrical contacts made only onto the Pt layer (see Methods) [16]. The device is mounted onto a rf waveguide,

and two dc electrodes are connected to the two sides of the Pt layer to measure the magnon spin current injected into Pt through inverse spin Hall effect (ISHE) [18–21]. As shown in Fig. 3(b), spin-pumping signals are observed under the driving rf frequencies between 3 and 9 GHz. By plotting the relationship between rf frequency and resonance field, we identify that the detected resonance signal corresponds to the contribution from the Py layer. This is further verified with separate ferromagnetic resonance measurements, where no obvious resonance peaks are observed from the YIG layer due to its polycrystalline nature (see Sec. 7 within the Supplemental Material) [16]. Moreover, a large dc resistance (up to 100 M $\Omega$ , see Fig. S6 within the Supplemental Material) [16] is measured between the

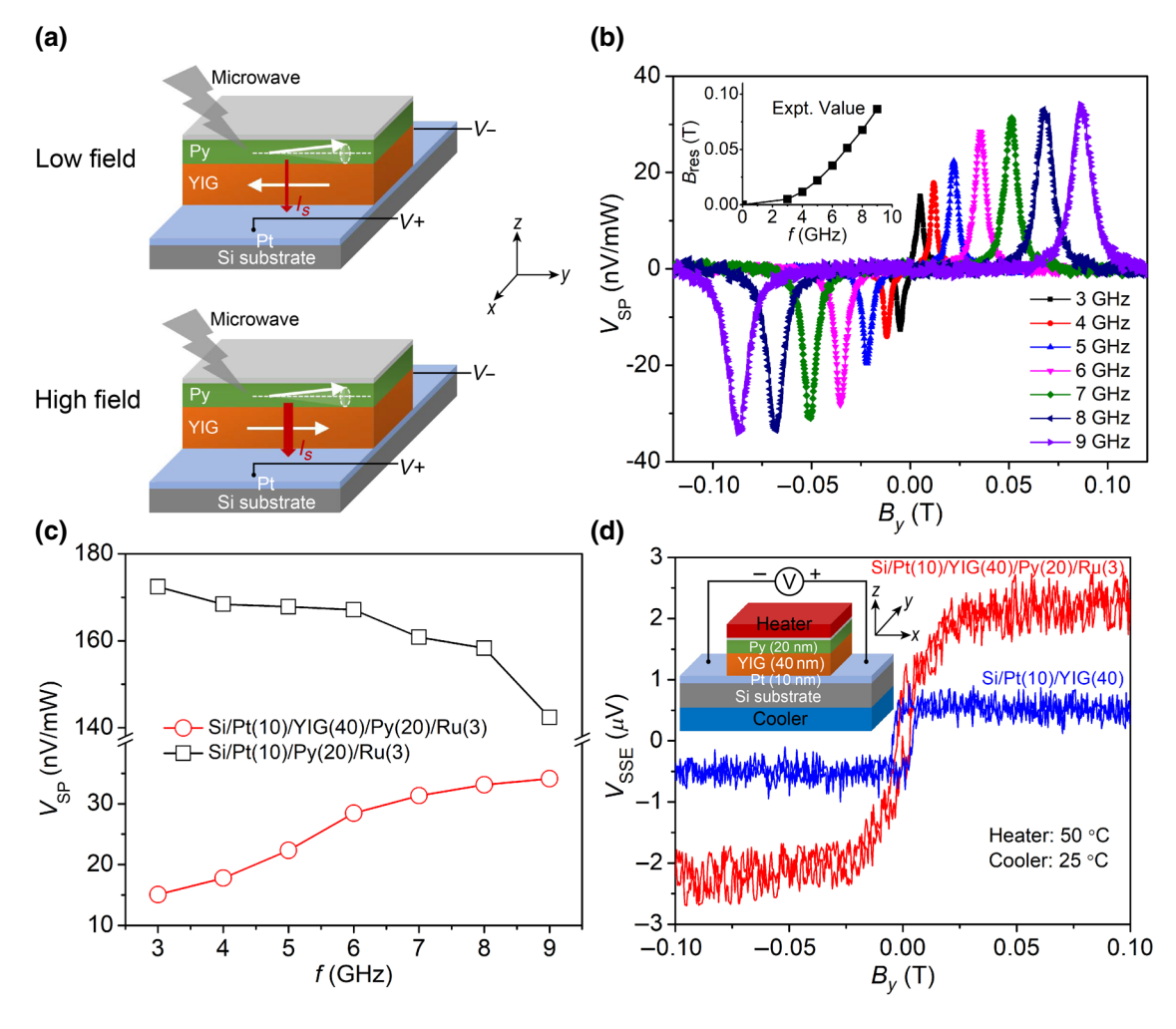


FIG. 3. (a) Schematics of the Py spin-pumping process when the Py and the YIG magnetizations are in the antiparallel (upper panel) and parallel (lower panel) configurations under the low-field and high-field regimes, respectively. (b) Spin-pumping voltages measured from the ISHE in the Pt layer when the Py magnetization is excited to ferromagnetic resonance by external rf field in the Si/Pt(10)/YIG(40)/Py(20)/Ru(3) hybrid structure. The spin-pumping voltages are normalized by the microwave power under different frequencies. Inset: resonance field versus frequency. (c) Comparison of the field-dependent spin-pumping voltages measured in the Si/Pt(10)/YIG(40)/Py(20)/Ru(3) structure and the control structure of Si/Pt(10)/Py(20)/Ru(3). (d) Spin-Seebeck voltages measured in the Si/Pt(10)/YIG(40)/Py(20)/Ru(3) hybrid structure, when the top Py(20)/Ru(3) is in contact with a ceramic electrical heater (maintained at 50 °C) and the bottom substrate is attached to a Peltier cooler (maintained at 25 °C). Spin-Seebeck data measured in a Si/Pt(10)/YIG(40) control sample is also plotted.

Py/Ru top layer and the Pt underlayer in our experiment, suggesting that the thick YIG layer can completely isolate the direct electrical current flow from Py to Pt. This allows us to exclude additional contributions from the rf rectification effect within the Py layer [22–24]. Therefore, the obtained signals can be directly attributed to the spin-pumping mechanism without relying on detailed analysis of the resonance lineshape [25].

We characterize the spin-pumping signal as a function of the rf signal frequency (or equivalently, the resonance field  $B_{\rm res}$ ). We note that under the lowest applied field (rf frequency f = 3 GHz), the spin-pumping voltage  $V_{\rm SP}$  remains small. With the increase of f (from 3 to 9 GHz) and  $B_{\rm res}$ ,  $V_{\rm SP}$  increases from 15 to 34.2 nV/mW. To understand the evolution of  $V_{SP}$ , we carry out a control experiment on a simple Pt/Py bilayer film. As is illustrated in Fig. 3(c), a different trend has been observed in the Pt/Py sample, where  $V_{\rm SP}$  decreases with the increase of resonance frequency. This latter trend is also consistent with previous reports [26–28] in similar spin-pumping experiments, which can be explained by the reduction of precession cone angle under a higher driven frequency (or equivalently, a larger external magnetic field). The observed monotonic increase of  $V_{\rm SP}$  as a function of frequency in Si/Pt/YIG/Py hybrid structure is consistent with the magnon spin-valve mechanism as schematically illustrated in Fig. 3(a), where the antiparallel configuration between the two magnetic layers blocks part of the magnon spin transport by lowering the spin transmission coefficient at the interface.

In addition to the spin-pumping experiment, we carry out spin-Seebeck-effect measurements in which a temperature gradient of 25 K is created along the vertical direction in the Si/Pt/YIG/Py structure. As plotted in Fig. 3(d), the spin-Seebeck voltage  $V_{\rm SSE}$  detected in the Pt layer increases monotonically with the in-plane magnetic field from 0 to 0.1 T, consistent with the scenario that the parallel configuration between Py and YIG magnetizations allows more magnon transmission from Py through the YIG layer than the antiparallel case. Importantly, we notice that even in the low-field regime (from 0 to 50 mT), where Py and YIG are mostly antiparallel, the  $V_{\rm SSE}$  in Pt/YIG/Py is greater than the  $V_{\rm SSE}$  measured in a Pt/YIG control sample, suggesting that magnons generated from the Py layer dominate.

The measured antiferromagnetic coupling between Py and YIG corresponds to an interfacial exchange energy of approximately  $8.6 \times 10^{-4}$  J/m<sup>2</sup>, which is orders of magnitude stronger than the value reported in single-crystal YIG/Py hybrid structure [29]. The strong intrinsic antiferromagnetic coupling between Py and YIG layers in our structure directly facilitates the realization of magnonic spin-valve effect. The elimination of extra spacer layers avoids additional spin scattering during magnon conversions, which not only enhances the efficiency but

also removes the constraints set by the spacer layer, such as antiferromagnetic Néel transition temperature [30–32]. In our spin-pumping experiment, the magnonic spin-valve effect can be evaluated as  $(V_{\rm SP}^{\uparrow\uparrow} - V_{\rm SP}^{\uparrow\downarrow})/V_{\rm SP}^{\uparrow\downarrow} = 130\%$ , which is comparable to the value measured in the YIG/CoO/Co structure reported previously [9], except that our measurement is carried out at room temperature while previous results are obtained under 160 K. In our experiment, the magnon spin valve switches under high and low magnetic field. Further nanoscale fabrication can introduce shape anisotropy into the magnetic layers, which will allow the realization of bistability between the parallel and antiparallel states and work as a nonvolatile switch. The fact that the magnonic spin valve operates efficiently at room temperature and it can be integrated with other Si-based electronics suggests that this material system can provide a nice platform for realizing magnon-based spin logic and memory devices. Additional references cited within the Supplemental Material are included here [33–35].

Acknowledgments. We thank Julie Borchers for invaluable discussions. This work is supported in part by the National Science Foundation under Grant No. ECCS-1808826 and by SMART, one of seven centers of nCORE, a Semiconductor Research Corporation program, sponsored by National Institute of Standards and Technology (NIST). The authors also acknowledge support from AFOSR under award FA9550-19-1-0048. P.Q. acknowledges support from the National Research Council Research Associateship Program. Research performed in part at the NIST Center for Nanoscale Science and Technology.

- [1] S. Klingler, V. Amin, S. Geprägs, K. Ganzhorn, H. Maier-Flaig, M. Althammer, H. Huebl, R. Gross, R. D. McMichael, M. D. Stiles, S. T. B. Goennenwein, and M. Weiler, Spin-Torque excitation of perpendicular standing spin waves in coupled YIG/Co heterostructures, Phys Rev. Lett. 120, 127201 (2018).
- [2] J. Chen, C. Liu, T. Liu, Y. Xiao, K. Xia, G. E. W. Bauer, M. Wu, and H. Yu, Strong Interlayer Magnon-Magnon Coupling in Magnetic Metal-Insulator Hybrid Nanostructures, Phys. Rev. Lett. 120, 217202 (2018).
- [3] H. Qin, S. J. Hämäläinen, and S. van Dijken, Exchange-torque-induced excitation of perpendicular standing spin waves in nanometer-thick YIG films, Sci. Rep. 8, 5755 (2018).
- [4] A. V. Chumak, A. A. Serga, and B. Hillebrands, Magnon transistor for all-magnon data processing, Nat. Commun. 5, 4700 (2014).
- [5] A. Khitun, M. Bao, and K. L. Wang, Magnonic logic circuits, J. Phys. D: Appl. Phys. 43, 264005 (2010).
- [6] Y. Tabuchi, S. Ishino, A. Noguchi, T. Ishikawa, R. Yamazaki, K. Usami, and Y. Nakamura, Coherent coupling

- between a ferromagnetic magnon and a superconducting qubit, Science 349, 405 (2015).
- [7] A. V. Chumak, V. I. Vasyuchka, A. A. Serga, and B. Hillebrands, Magnon spintronics, Nat. Phys. 11, 453 (2015).
- [8] H. Wu, L. Huang, C. Fang, B. S. Yang, C. H. Wan, G. Q. Yu, J. F. Feng, H. X. Wei, and X. F. Han, Magnon Valve Effect Between Two Magnetic Insulators, Phys. Rev. Lett. 120, 097205 (2018).
- [9] J. Cramer, F. Fuhrmann, U. Ritzmann, V. Gall, T. Niizeki, R. Ramos, Z. Qiu, D. Hou, T. Kikkawa, J. Sinova, U. Nowak, E. Saitoh, and M. Kläui, Magnon detection using a ferroic collinear multilayer spin valve, Nat. Commun. 9, 1089 (2018).
- [10] J. S. Moodera, L. R. Kinder, T. M. Wong, and R. Meservey, Large Magnetoresistance at Room Temperature in Ferromagnetic Thin Film Tunnel Junctions, Phys. Rev. Lett. 74, 3273 (1995).
- [11] T. Miyazaki and N. Tezuka, Giant magnetic tunneling effect in Fe/Al<sub>2</sub>O<sub>3</sub>/Fe junction, J. Magn. Magn. Mater. 139, L231 (1995).
- [12] T. Liu, H. Chang, V. Vlaminck, Y. Sun, M. Kabatek, A. Hoffmann, L. Deng, and M. Wu, Ferromagnetic resonance of sputtered yttrium iron garnet nanometer films, J. Appl. Phys. 115, 17A501 (2014).
- [13] H. Chang, P. Li, W. Zhang, T. Liu, A. Hoffmann, L. Deng, and M. Wu, Nanometer-Thick yttrium iron garnet films With extremely Low damping, IEEE Magn. Lett. 5, 1 (2014).
- [14] H. Chang, T. Liu, D. R. Hickey, P. A. P. Janantha, K. A. Mkhoyan, and M. Wu, Sputtering growth of Y<sub>3</sub>Fe<sub>5</sub>O<sub>12</sub>/Pt bilayers and spin transfer at Y<sub>3</sub>Fe<sub>5</sub>O<sub>12</sub>/Pt interfaces, APL Mater. 5, 126104 (2017).
- [15] H. Wu, C. H. Wan, X. Zhang, Z. H. Yuan, Q. T. Zhang, J. Y. Qin, H. X. Wei, X. F. Han, and S. Zhang, Observation of magnon-mediated electric current drag at room temperature, Phys. Rev. B 93, 060403 (2016).
- [16] See Supplemental Material at http://link.aps.org/supplemental/10.1103/PhysRevApplied.13.061002 for complete PNR dataset, and control measurements using PNR, transport, FMR, and spin pumping.
- [17] B. J. Kirby, P. A. Kienzle, B. B. Maranville, N. F. Berk, J. Krycka, F. Heinrich, and C. F. Majkrzak, Phase-sensitive specular neutron reflectometry for imaging the nanometer scale composition depth profile of thin-film materials, Curr. Opin. Colloid Interface Sci. 17, 44 (2012).
- [18] Y. Tserkovnyak, A. Brataas, and G. E. W. Bauer, Enhanced Gilbert Damping in Thin Ferromagnetic Films, Phys. Rev. Lett. 88, 117601 (2002).
- [19] Y. Kajiwara, K. Harii, S. Takahashi, J. Ohe, K. Uchida, M. Mizuguchi, H. Umezawa, H. Kawai, K. Ando, K. Takanashi, S. Maekawa, and E. Saitoh, Transmission of electrical signals by spin-wave interconversion in a magnetic insulator, Nature 464, 262 (2010).
- [20] C. W. Sandweg, Y. Kajiwara, A. V. Chumak, A. A. Serga, V. I. Vasyuchka, M. B. Jungfleisch, E. Saitoh, and B. Hillebrands, Spin Pumping by Parametrically Excited Exchange Magnons, Phys. Rev. Lett. 106, 216601 (2011).
- [21] H. L. Wang, C. H. Du, Y. Pu, R. Adur, P. C. Hammel, and F. Y. Yang, Large spin pumping from epitaxial Y<sub>3</sub>Fe<sub>5</sub>O<sub>12</sub> thin films to Pt and W layers, Phys. Rev. B 88, 100406 (2013).

- [22] L. Bai, P. Hyde, Y. S. Gui, C. M. Hu, V. Vlaminck, J. E. Pearson, S. D. Bader, and A. Hoffmann, Universal Method for Separating Spin Pumping From Spin Rectification Voltage of Ferromagnetic Resonance, Phys. Rev. Lett. 111, 217602 (2013).
- [23] Y. S. Gui, N. Mecking, X. Zhou, G. Williams, and C. M. Hu, Realization of a Room-Temperature Spin Dynamo: The Spin Rectification Effect, Phys. Rev. Lett. 98, 107602 (2007).
- [24] A. Azevedo, L. H. Vilela-Leão, R. L. Rodríguez-Suárez, A. F. Lacerda Santos, and S. M. Rezende, Spin pumping and anisotropic magnetoresistance voltages in magnetic bilayers: Theory and experiment, Phys. Rev. B 83, 144402 (2011).
- [25] O. Mosendz, J. E. Pearson, F. Y. Fradin, G. E. W. Bauer, S. D. Bader, and A. Hoffmann, Quantifying Spin Hall Angles From Spin Pumping: Experiments and Theory, Phys. Rev. Lett. 104, 046601 (2010).
- [26] K. Harii, T. An, Y. Kajiwara, K. Ando, H. Nakayama, T. Yoshino, and E. Saitoh, Frequency dependence of spin pumping in Pt/Y<sub>3</sub>Fe<sub>5</sub>O<sub>12</sub> film, J. Appl. Phys. 109, 116105 (2011).
- [27] H. Wang, J. Kally, J. S. Lee, T. Liu, H. Chang, D. R. Hickey, K. A. Mkhoyan, M. Wu, A. Richardella, and N. Samarth, Surface-State-Dominated Spin-Charge Current Conversion in Topological-Insulator-Ferromagnetic-Insulator Heterostructures, Phys. Rev. Lett. 117, 076601 (2016).
- [28] X. Tao, Q. Liu, B. Miao, R. Yu, Z. Feng, L. Sun, B. You, J. Du, K. Chen, S. Zhang, L. Zhang, Z. Yuan, D. Wu, and H. Ding, Self-consistent determination of spin hall angle and spin diffusion length in Pt and Pd: The role of the interface spin loss, Sci. Adv. 4, eaat1670 (2018).
- [29] K. S. Das, W. Y. Schoemaker, B. J. van Wees, and I. J. Vera-Marun, Spin injection and detection via the anomalous spin hall effect of a ferromagnetic metal, Phys. Rev. B **96**, 220408 (2017).
- [30] Z. Qiu, D. Hou, J. Barker, K. Yamamoto, O. Gomonay, and E. Saitoh, Spin colossal magnetoresistance in an antiferromagnetic insulator, Nat. Mater. 17, 577 (2018).
- [31] Q. Li, M. Yang, C. Klewe, P. Shafer, A. T. N'Diaye, D. Hou, T. Y. Wang, N. Gao, E. Saitoh, C. Hwang, R. J. Hicken, J. Li, E. Arenholz, and Z. Q. Qiu, Coherent ac spin current transmission across an antiferromagnetic CoO insulator, Nat. Commun. 10, 5265 (2019).
- [32] Z. Qiu, J. Li, D. Hou, E. Arenholz, A. T. N'Diaye, A. Tan, K.-I. Uchida, K. Sato, S. Okamoto, Y. Tserkovnyak, Z. Q. Qiu, and E. Saitoh, Spin-current probe for phase transition in an insulator, Nat. Commun. 7, 12670 (2016).
- [33] P. A. Kienzle, https://www.nist.gov/ncnr/reflectometry-so ftware (2017).
- [34] B. Maranville, W. Ratcliff II, and P. Kienzle, Reductus: a stateless Python data reduction service with a browser front end, J. Appl. Crystallogr. **51**, 1500 (2018).
- [35] C. F. Majkrzak, C. Metting, B. B. Maranville, J. A. Dura, S. Satija, T. Udovic, and N. F. Berk, Determination of the effective transverse coherence of the neutron wave packet as employed in reflectivity investigations of condensed-matter structures. I. measurements, Phys. Rev. A 89, 033851 (2014).